Non-boost-invariant anisotropic dynamics

Mauricio Martinez[a,c], Michael Strickland[b,c]

[a] *Institut für Theoretische Physik*
Goethe-Universität Frankfurt
Max-von-Laue Strasse 1
D-60438, Frankfurt am Main, Germany
[b] *Physics Department, Gettysburg College*
Gettysburg, PA 17325 United States
[c] *Frankfurt Institute for Advanced Studies*
Ruth-Moufang-Strasse 1
D-60438, Frankfurt am Main, Germany

Abstract

We study the non-boost-invariant evolution of a quark-gluon plasma subject to large early-time momentum-space anisotropies. Rather than using the canonical hydrodynamical expansion of the distribution function around an isotropic equilibrium state, we expand around a state which is anisotropic in momentum space and parameterize this state in terms of three proper-time and spatial-rapidity dependent parameters. Deviations from the Bjorken scaling solutions are naturally taken into account by the time evolution of the spatial-rapidity dependence of the anisotropic ansatz. As a result, we obtain three coupled partial differential equations for the momentum-space anisotropy, the typical momentum of the degrees of freedom, and the longitudinal flow. Within this framework (0+1)-dimensional Bjorken expansion is obtained as an asymptotic limit. Finally, we make quantitative comparisons of the temporal and spatial-rapidity evolution of the dynamical parameters and resulting pressure anisotropy in both the strong and weak coupling limits.

Keywords: Non-Boost-Invariant Dynamics, Anisotropic Plasma, Non-equilibrium Evolution, Viscous Hydrodynamics.

1. Introduction

In recent years relativistic viscous hydrodynamical models have been applied with great success to the description of the non-central anisotropic flow measured at the Relativistic Heavy Ion Collider [1–8]. Despite this success, it is well known viscous hydrodynamics is not an accurate description during early times after the initial impact. The hot and dense matter created after the collision is rather small in transverse extent and expands very rapidly in the longitudinal direction. In addition, transverse expansion of the matter is not expected to become important until times on the order of 3 or 4 fm/c after the collision. As a consequence, large momentum-space anisotropies are developed at early-times. When these anisotropies are large the shear viscous corrections can be of the same order or larger than

the isotropic pressure, casting doubt on the validity of viscous hydrodynamics to faithfully model the dynamics. For example, it is known that within the framework of 2nd-order viscous hydrodynamics large momentum-space anisotropies can lead to negative longitudinal pressure at early times [9].

One is therefore motivated to develop an alternative approach that will allow us to better understand the transition between early-time anisotropic expansion and late-time hydrodynamical behaviour in ultrarelativistic heavy ion collisions. The work presented here fills this gap using a technique which allows one to smoothly connect both regimes using a unified theoretical framework. We present a method which allows us to derive hydrodynamical-like evolution equations in the presence of large momentum-space anisotropies. The method consists of changing the usual hydrodynamic expansion of the one-particle distribution function in the local rest frame

$$f(\mathbf{x},\mathbf{p},\tau) = f_{\rm eq}(|\mathbf{p}|,T(\tau)) + \delta f_1 + \delta f_2 + \cdots \ , \tag{1}$$

which is an expansion around an isotropic equilibrium state $f_{\rm eq}(|\mathbf{p}|,T)$, to one in which the expansion point itself can contain momentum-space anisotropies

$$f(\mathbf{x},\mathbf{p},\tau) = f_{\rm aniso}(\mathbf{p},p_{\rm hard},\xi) + \delta f_1' + \delta f_2' + \cdots \ . \tag{2}$$

In Eq. (2) ξ is a parameter that measures the amount of momentum-space anisotropy and $p_{\rm hard}$ is a non-equilibrium momentum scale which can be identified with the temperature of the system only in the limit of isotropic equilibrium. We introduce an ansatz for the leading order term of Eq. (2), $f_{\rm aniso}(\mathbf{p},p_{\rm hard},\xi)$, which approximates the system via spheroidal equal occupation number surfaces as opposed to the spherical ones associated with the isotropic equilibrium distribution function [10]. We do not calculate the remaining terms of the corrections $\delta f_n'$, their evaluation is beyond the scope of this paper. Nevertheless, it may be possible to perform such a calculation in a consistent way for relativistic system with the use of irreducible anisotropic tensors [11] or spheroidal harmonics [12] for which our ansatz is the leading order term. Moreover, one expects that the corrections $\delta f_n'$ will have smaller magnitude than the isotropic corrections δf_n because of the momentum-space anisotropy is built into the leading order term in the reorganized expansion.

In this paper we extend our previous work on highly anisotropic dynamics [13] to include both temporal and spatial-rapidity dependence of the system thereby removing the assumption of boost invariance of the system. By making use of an ansatz for $f_{\rm aniso}(\mathbf{p},p_{\rm hard},\xi)$, we derive leading order evolution equations for a non-boost-invariant plasma which expands only in the longitudinal direction. Based on this ansatz we obtain three coupled partial differential equations for the momentum-space anisotropy, the typical momentum scale of the particles and the longitudinal flow rapidity. We show that these equations reduce to the boost-invariant description of the plasma in the appropriate limit. Finally, we present numerical solutions of the non-boost-invariant evolution equations and make a quantitative description of the pressure anisotropy for weak and strong coupling.

2. Kinetic theory approach for a non-boost-invariant and highly anisotropic QGP

In this section we derive the equations of motion necessary to describe the transition between early time dynamics and late-time hydrodynamical behaviour of a non-boost-invariant system. For simplicity, we assume that there is no transverse expansion and that all expansion is along the longitudinal direction.[1] The derivation is based on taking moments of the Boltzmann equation. Before presenting the evolution equations, we first review the moment method of the Boltzmann equation applied to general relativistic theories [15–17], then we apply this formalism to the case of a non-boost-invariant system which is anisotropic in momentum space.

2.1. Moments of the Boltzmann equation

For a dilute system, the Boltzmann relativistic transport equation for the on-shell phase space density $f(\mathbf{x}, \mathbf{p}, t)$ is [15]

$$p^\mu \partial_\mu f(\mathbf{x}, \mathbf{p}, t) = -\mathcal{C}\big[f\big]\,, \tag{3}$$

where $\mathcal{C}\big[f\big]$ is the collisional kernel which is a functional of the distribution function. In order to have a tractable approach to dissipative dynamics from kinetic theory, one usually takes moments of the Boltzmann equation (3) to determine the equations of motion of the dissipative currents [15–17].

The equation of motion for the n-th moment of the Boltzmann equation is[2]

$$\partial_{\mu_{n+1}} I^{\mu_1 \mu_2 \cdots \mu_{n+1}} = -P^{\mu_1 \mu_2 \cdots \mu_n}\,, \tag{4}$$

where

$$I^{\mu_1 \mu_2 \cdots \mu_{n+1}} = \int_{\mathbf{p}} p^{\mu_1} p^{\mu_2} \ldots p^{\mu_{n+1}}\, f(\mathbf{x}, \mathbf{p}, t)\,, \tag{5a}$$

$$P^{\mu_1 \mu_2 \cdots \mu_n} = \int_{\mathbf{p}} p^{\mu_1} p^{\mu_2} \ldots p^{\mu_n}\, \mathcal{C}\big[f\big]\,. \tag{5b}$$

Eq. (4) defines an infinite set of coupled equations for these moments. By truncating the expansion, one obtains a finite set of equations [15]. In the Israel-Stewart (IS) theory, the evolution equation for the dissipative currents and the transport coefficients can be extracted from the second moment of the Boltzmann equation within the 14 Grad's ansatz for the distribution function [16, 17].

[1] We point out that the method presented here can be generalized to include azimuthal and non-azimuthal transverse expansion. We postpone these studies to a future publication [14].

[2] Our notation for the momentum-space integral is $\int_{\mathbf{p}} \equiv (2\pi)^{-3} \int d^3\mathbf{p}/p^0$.

By using Eq. (4) for $n = 0, 1, 2$; one finds

$$\int_{\mathbf{p}} p^\mu \partial_\mu f(x,p) \equiv \partial_\mu N^\mu = \int_{\mathbf{p}} \mathcal{C}[f] \,, \tag{6a}$$

$$\int_{\mathbf{p}} p^\mu p^\nu \partial_\mu f(x,p) \equiv \partial_\mu T^{\mu\nu} = \int_{\mathbf{p}} p^\nu \mathcal{C}[f] \equiv 0 \,, \tag{6b}$$

$$\int_{\mathbf{p}} p^\mu p^\nu p^\lambda \partial_\mu f(x,p) \equiv \partial_\mu I^{\mu\nu\lambda} = \int_{\mathbf{p}} p^\nu p^\lambda \mathcal{C}[f] \equiv P^{\nu\lambda} \,. \tag{6c}$$

The zeroth moment of the Boltzmann equation (6a), tells us the evolution of the particle current N^μ. When $\int_{\mathbf{p}} \mathcal{C}[f] = 0$, we have particle number conservation, however, for general gauge theories like QCD where inelastic processes are important, away from chemical equilibrium we have $\int_{\mathbf{f}} \mathcal{C}[f] \neq 0$, i.e. there is a source term for particle production and annihilation [18–21]. The first moment of the Boltzmann equation (6b), gives us the conservation of the energy and momentum since $\int_{\mathbf{p}} p^\mu \mathcal{C}[f] = 0$. Eq. (6c) represents the balance of the dissipative fluxes. $I^{\mu\nu\lambda}$ is a symmetric tensor of the dissipative fluxes and $P^{\nu\lambda}$ is a traceless tensor that is related to dissipative processes due to collisions [15, 17, 22]. The right hand side of Eq. (6c) does not trivially vanish, so in general $\int_{\mathbf{p}} p^\nu p^\lambda \mathcal{C}[f] \equiv P^{\nu\lambda} \neq 0$.

To obtain the complete set of equations for the dynamical variables such as the particle density n, energy density $\mathcal{E}$, etc., in hydrodynamical treatments one canonically expands the distribution function around equilibrium by using some functional form for the fluctuations (see Eq. (1)). In our approach, we do not expand the distribution function around an isotropic expansion point. Instead, we find evolution equations for the kinematical parameters contained in the leading term f_{aniso} in Eq. (2) by taking moments of the Boltzmann equation.

2.2. Energy-momentum tensor for a highly anisotropic plasma

The general energy-momentum tensor for an anisotropic plasma is given by [23, 24]

$$T^{\mu\nu} = (\mathcal{E} + \mathcal{P}_T)\, u^\mu u^\nu - \mathcal{P}_T\, g^{\mu\nu} - (\mathcal{P}_T - \mathcal{P}_L) v^\mu v^\nu \,, \tag{7}$$

where $\mathcal{E}$, $\mathcal{P}_T$, and $\mathcal{P}_L$ are the energy density, transverse pressure, and longitudinal pressure. u^μ is a unitary four-vector which defines the longitudinal flow velocity of the system. In the local rest frame (LRF), $u^\mu = (1, 0, 0, 0)$. In addition to the fluid velocity, we introduce a vector v^μ that is a normalized space-like vector ($v^\mu v_\mu = -1$) which is orthogonal to u^μ ($u_\mu v^\mu = 0$). In the LRF, $v^\mu = (0, 0, 0, 1)$.[3]

The energy momentum tensor takes a diagonal form $T^{\mu\nu} = \text{diag}(\mathcal{E}, \mathcal{P}_T, \mathcal{P}_T, \mathcal{P}_L)$ in the LRF. The evolution of its components are given by energy-momentum conservation

$$\partial_\mu T^{\mu\nu} = 0 \,. \tag{8}$$

[3]Usually in hydrodynamics, one uses operator $\Delta^{\mu\nu} = g^{\mu\nu} - u^\mu u^\nu$ which is orthogonal to the four-velocity u^μ. From its definition, it is straightforward to see that v^μ is an eigenvector of the operator $\Delta^{\mu\nu}$ with eigenvalue equal to one, i.e. $\Delta^{\mu\nu} v_\nu = v^\mu$.

If we project the last expression with u^μ and v^μ we obtain [24]

$$\mathcal{D}\mathcal{E} = -\big(\mathcal{E}+\mathcal{P}_T\big)\theta + \big(\mathcal{P}_T-\mathcal{P}_L\big)u_\mu\bar{\mathcal{D}}v^\mu\,, \tag{9a}$$

$$\bar{\mathcal{D}}\mathcal{P}_L = -\big(\mathcal{P}_T-\mathcal{P}_L\big)\bar{\theta} + \big(\mathcal{E}+\mathcal{P}_T\big)v_\mu\mathcal{D}u^\mu\,, \tag{9b}$$

where $\mathcal{D} = u^\mu\partial_\mu$, $\bar{\mathcal{D}} = v^\mu\partial_\mu$, $\theta = \partial_\mu u^\mu$ and $\bar{\theta} = \partial_\mu v^\mu$.

2.3. Boltzmann equation for the anisotropic distribution function

In order to make analytical progress, we will assume that the leading term of Eq. (2) is given by the ansatz proposed by Romatschke and Strickland [10]. Within this approach the leading order anisotropic distribution function in the LRF can be obtained from an arbitrary isotropic distribution function ($f_{\rm iso}$) by squeezing or stretching $f_{\rm iso}$ along one direction in momentum space

$$f(\mathbf{x},\mathbf{p},\tau) = f_{\rm iso}\big(p_\mu p_\nu \xi^{\mu\nu}(x)/p^2_{\rm hard}(x)\big)\,, \tag{10}$$

where $p_{\rm hard}$ is related to the average momentum of the partons and $\xi^{\mu\nu}(x)$ is a symmetric tensor which indicates the direction and strength of the anisotropy. This particular choice is a generalization of the original longitudinal RS ansatz [10].

In this work we restrict ourselves to a system which expands along the longitudinal direction in a non-boost-invariant way so that $\xi^{\mu\nu}$ takes the form

$$\xi^{\mu\nu}(x) = \mathrm{diag}(1,0,0,\xi(x)), \tag{11}$$

where $-1<\xi<\infty$ is a parameter that reflects the strength and type of anisotropy. [4] Using this, the first argument of Eq. (10) becomes

$$\begin{aligned}\xi^{\mu\nu}(x)\,p_\mu p_\nu &= (p_0)^2 + \xi p_z^2\,,\\ &= p_T^2 + (1+\xi)p_z^2\,,\end{aligned} \tag{12}$$

where we have considered on-shell massless particles and $p_T^2 = p_x^2+p_y^2$. Choosing $\xi^{\mu\nu}$ as given by (11) allows us to recover the original form of the RS ansatz as used by the authors of Ref. [10], i.e.

$$f(\mathbf{x},\mathbf{p},\tau) = f_{\rm RS}(\mathbf{p},\xi,p_{\rm hard}) = f_{\rm iso}([\mathbf{p}_T^2+(1+\xi)p_z^2]/p^2_{\rm hard})\,. \tag{13}$$

To write the non-boost-invariant Boltzmann equation for the RS ansatz (13), it is convenient to switch to the coordinates specified by $\tau=\sqrt{t^2-z^2}$ and $\tanh\varsigma = z/t$. In this coordinate system, the RS ansatz (13) is

$$f_{\rm RS}(\mathbf{p},\xi,p_{\rm hard},\vartheta) = f_{\rm iso}\big(\mathbf{p}_T^2[1+(1+\xi)\sinh^2(y-\vartheta)]/p^2_{\rm hard}\big)\,, \tag{14}$$

[4] The anisotropy parameter ξ is related to the average longitudinal and transverse momentum of the plasma partons via the relation [25, 26] $\xi = \frac{1}{2}\langle p_T^2\rangle/\langle p_L^2\rangle - 1$. The system is locally isotropic when $\xi = 0$.

where ϑ is the hyperbolic angle associated with the comoving or LRF and y is the lab momentum-space rapidity. Note that ξ, $p_{\rm hard}$ and ϑ are functions of both τ and ς. After changing variables, the Boltzmann equation is

$$\left(p_T \cosh(y-\vartheta)\frac{\partial}{\partial\tau} + \frac{p_T \sinh(y-\vartheta)}{\tau}\frac{\partial}{\partial\varsigma}\right) f_{\rm RS}(\mathbf{p},\xi,p_{\rm hard},\vartheta) = -\mathcal{C}[f_{\rm RS}]\,. \tag{15}$$

So far we have not prescribed a specific collisional kernel $\mathcal{C}[f]$. Since the calculation of the collisional kernel is difficult in general, we model it here by considering the relaxation time approximation

$$\mathcal{C}[f_{RS}] = p_\mu u^\mu \,\Gamma\, \left[f_{\rm RS}(\mathbf{p},\xi,p_{\rm hard},\vartheta) - f_{\rm eq}(|\mathbf{p}|,T)\right]\,, \tag{16}$$

where $f_{\rm eq}(|\mathbf{p}|,T)$ is the local equilibrium distribution and Γ is the relaxation rate. The temperature T is determined dynamically by requiring energy conservation $\mathcal{E}_{\rm eq}(\tau) = \mathcal{E}_{\text{non-eq}}(\tau)$ [13, 27]. From the results of Appendix A one finds for the RS ansatz (13) that $T = R^{1/4}(\xi)p_{\rm hard}$ [13, 28]. As we demonstrated in a previous paper [13], Γ can be related to the shear viscosity and shear relaxation time of the system by matching our treatment to 2nd-order viscous hydrodynamics in the small anisotropy limit. We will return to this point in the end of the next section.

2.4. Evolution equations for the kinematical parameters of the RS ansatz

In this section we apply the moment method to the anisotropic RS ansatz (13) for a non-boost-invariant system. The boost invariant case was already studied in a previous publication [13]. We will assume in what follows that the system is conformal and therefore $\mathcal{E}_{\rm iso} = 3\mathcal{P}_{\rm iso}$.

2.4.1. 0th moment of the non-boost invariant Boltzmann equation

As we mentioned in Sect. 2.1, the 0th moment of the Boltzmann equation is equivalent to the equation for the evolution of the particle current N^μ (Eq. (6a)). After plugging the RS ansatz (13) into the Boltzmann equation, the left hand side (LHS) of Eq. (15) is

$$\begin{aligned}\text{LHS} \;=\; \partial_\omega f_{\rm iso}(\omega)\Big[&\frac{p_z^2}{p_{\rm hard}^2}\Big(E\,\partial_\tau\xi + \frac{p_z}{\tau}\partial_\varsigma\xi\Big) - \frac{2\,E\,p_z}{p_{\rm hard}^2}\,(1+\xi)\,\Big(E\,\partial_\tau\vartheta + \frac{p_z}{\tau}\partial_\varsigma\vartheta\Big)\\ &-\frac{2\omega}{p_{\rm hard}}\Big(E\,\partial_\tau p_{\rm hard} + \frac{p_z}{\tau}\partial_\varsigma p_{\rm hard}\Big)\Big]\,,\end{aligned} \tag{17}$$

where $\omega \equiv \left[p_T^2 + (1+\xi)p_z^2\right]/p_{\rm hard}^2$ and we have rewritten the result in terms of the energy and longitudinal momentum in the LRF defined in the fluid cell via $E = p_T\cosh(y-\vartheta)$ and $p_z = p_T\sinh(y-\vartheta)$, respectively. Taking the zeroth moment (integrating over the momentum-space measure $(2\pi)^{-3}\int d^3\mathbf{p}/E$) of the last expression together with the right

hand side of Eq. (15), we obtain

$$\frac{\left\langle p_z^2\,\partial_\omega f_{\rm iso}(\omega)\right\rangle}{p_{\rm hard}^2}\left(\partial_\tau\xi-\frac{2(1+\xi)}{\tau}\partial_\varsigma\vartheta\right)+\left\langle\frac{p_z^3}{E}\,\partial_\omega f_{\rm iso}(\omega)\right\rangle\frac{\partial_\varsigma\xi}{\tau\,p_{\rm hard}^2}$$
$$-2\left\langle E\,p_z\,\partial_\omega f_{\rm iso}(\omega)\right\rangle\frac{(1+\xi)}{p_{\rm hard}^2}\,\partial_\tau\vartheta-2\,\frac{\left\langle\omega\,\partial_\omega f_{\rm iso}(\omega)\right\rangle}{p_{\rm hard}}\,\partial_\tau p_{\rm hard}$$
$$-\frac{2\left\langle\omega\,p_z\,\partial_\omega f_{\rm iso}(\omega)\right\rangle}{p_{\rm hard}}\,\partial_\varsigma p_{\rm hard}=-\Gamma\Big[\left\langle f_{\rm iso}(\mathbf{p},\xi,p_{\rm hard})\right\rangle-\left\langle f_{\rm eq}\big(\mathbf{p},T(\tau)\big)\right\rangle\Big],\tag{18}$$

where $\langle a\rangle\equiv(2\pi)^{-3}\int d^3\mathbf{p}$. These integrals can be calculated analytically using the general form of the RS ansatz (13)

$$\left\langle p_z^2\,\partial_\omega f_{\rm iso}(\omega)\right\rangle=-\frac{1}{2}\frac{p_{\rm hard}^2}{(1+\xi)^{3/2}}\,n_{\rm iso}(p_{\rm hard})\,,\tag{19a}$$
$$\left\langle\frac{p_z^3}{E}\,\partial_\omega f_{\rm iso}(\omega)\right\rangle=0\,,\tag{19b}$$
$$\left\langle E\,p_z\,\partial_\omega f_{\rm iso}(\omega)\right\rangle=0\,,\tag{19c}$$
$$\left\langle\omega\,\partial_\omega f_{\rm iso}(\omega)\right\rangle=-\frac{3}{2}\,\frac{n_{\rm iso}(p_{\rm hard})}{(1+\xi)^{1/2}}\,,\tag{19d}$$
$$\left\langle\omega\,p_z\,\partial_\omega f_{\rm iso}(\omega)\right\rangle=0\,,\tag{19e}$$
$$\left\langle f_{\rm RS}(\mathbf{p},\xi,p_{\rm hard})\right\rangle=\frac{n_{\rm iso}(p_{\rm hard})}{(1+\xi)^{1/2}}\,,\tag{19f}$$
$$\left\langle f_{\rm eq}\big(\mathbf{p},T(\tau)=\mathcal{R}^{1/4}(\xi)p_{\rm hard}\big)\right\rangle=\mathcal{R}^{3/4}(\xi)\,n_{\rm iso}(p_{\rm hard})\,,\tag{19g}$$

where in the last line we have used the Landau matching condition $T(\tau)=\mathcal{R}^{1/4}(\xi)p_{\rm hard}$. After replacing these averages in Eq. (18), we obtain our first partial differential equation

$$\frac{1}{1+\xi}\Big(\partial_\tau\xi-\frac{2(1+\xi)}{\tau}\,\partial_\varsigma\vartheta\Big)-\frac{6}{p_{\rm hard}}\partial_\tau p_{\rm hard}=2\Gamma\left[1-\mathcal{R}^{3/4}(\xi)\sqrt{1+\xi}\right].\tag{20}$$

2.4.2. 1st moment of the non-boost invariant Boltzmann equation

In Sect. 2.1 we pointed out the equivalence between the first moment of the Boltzmann equation and energy-momentum conservation (Eq. (6b)). Therefore, we can use Eqs. (9) derived from the energy-momentum tensor given by (7). For the longitudinal dimension, it is useful to use the following parametrizations for the vectors u^μ and v^μ introduced in Sect. 2.2 [24, 29, 30]

$$u^\mu=(\cosh\vartheta(\tau,\varsigma),0,0,\sinh\vartheta(\tau,\varsigma))\,,\tag{21a}$$
$$v^\mu=(\sinh\vartheta(\tau,\varsigma),0,0,\cosh\vartheta(\tau,\varsigma))\,,\tag{21b}$$

where ϑ is the hyperbolic angle associated with the velocity of the LRF as measured in the lab frame. With this particular choice, one finds

$$u_\mu \bar{\mathcal{D}} v^\mu = \theta = \Big(\sinh(\vartheta-\varsigma)\,\partial_\tau + \frac{\cosh(\vartheta-\varsigma)}{\tau}\,\partial_\varsigma\Big)\vartheta\,, \tag{22}$$

$$v_\mu \mathcal{D} u^\mu = -\bar{\theta} = -\Big(\cosh(\vartheta-\varsigma)\,\partial_\tau + \frac{\sinh(\vartheta-\varsigma)}{\tau}\,\partial_\varsigma\Big)\vartheta\,. \tag{23}$$

Using these identities, in this coordinate system we can rewrite Eqs. (9) as[5]

$$\Big(\partial_\tau + \frac{\tanh(\vartheta(\tau,\varsigma)-\varsigma)}{\tau}\,\partial_\varsigma\Big)\mathcal{E}(\tau,\varsigma) = - \big(\mathcal{E}(\tau,\varsigma)+\mathcal{P}_L(\tau,\varsigma)\big)\Big(\tanh(\vartheta(\tau,\varsigma)-\varsigma)\,\partial_\tau + \frac{\partial_\varsigma}{\tau}\Big)\vartheta(\tau,\varsigma)\,, \tag{24a}$$

$$\Big(\tanh(\vartheta(\tau,\varsigma)-\varsigma)\partial_\tau + \frac{\partial_\varsigma}{\tau}\Big)\mathcal{P}_L(\tau,\varsigma) = - \big(\mathcal{E}(\tau,\varsigma)+\mathcal{P}_L(\tau,\varsigma)\big)\Big(\partial_\tau + \frac{\tanh(\vartheta(\tau,\varsigma)-\varsigma)}{\tau}\,\partial_\varsigma\Big)\vartheta(\tau,\varsigma)\,. \tag{24b}$$

Using the RS ansatz (13) it is possible to obtain analytic expressions for the energy density and longitudinal pressure (see Appendix A, Eqs. (A.1a) and (A.1c), respectively). Using these results, plugging them into Eqs. (24) and performing some algebra, we finally obtain the remaining two evolution equations

$$\frac{\mathcal{R}'(\xi)}{\mathcal{R}(\xi)}\,\partial_\tau\xi + 4\,\frac{\partial_\tau p_{\rm hard}}{p_{\rm hard}} + \frac{\tanh(\vartheta-\varsigma)}{\tau}\left(\frac{\mathcal{R}'(\xi)}{\mathcal{R}(\xi)}\,\partial_\varsigma\xi + 4\,\frac{\partial_\varsigma p_{\rm hard}}{p_{\rm hard}}\right) = -\Big(1+\frac{1}{3}\frac{\mathcal{R}_L(\xi)}{\mathcal{R}(\xi)}\Big)\Big(\tanh(\vartheta-\varsigma)\,\partial_\tau + \frac{\partial_\varsigma}{\tau}\Big)\vartheta\,, \tag{25a}$$

$$\tanh(\vartheta-\varsigma)\left(\frac{\mathcal{R}'_L(\xi)}{\mathcal{R}_L(\xi)}\,\partial_\tau\xi + 4\,\frac{\partial_\tau p_{\rm hard}}{p_{\rm hard}}\right) + \frac{1}{\tau}\left(\frac{\mathcal{R}'_L(\xi)}{\mathcal{R}_L(\xi)}\,\partial_\varsigma\xi + 4\,\frac{\partial_\varsigma p_{\rm hard}}{p_{\rm hard}}\right) = -\Big(3\,\frac{\mathcal{R}(\xi)}{\mathcal{R}_L(\xi)}+1\Big)\Big(\partial_\tau + \frac{\tanh(\vartheta-\varsigma)}{\tau}\,\partial_\varsigma\Big)\vartheta\,, \tag{25b}$$

where $\mathcal{R}(\xi)$ and $\mathcal{R}_L(\xi)$ are defined in Eqs. (A.1a) and (A.1c), respectively, while $\mathcal{R}'(\xi)$ and $\mathcal{R}'_L(\xi)$ are

$$\mathcal{R}'(\xi) = \partial_\xi\mathcal{R}(\xi) = \frac{1}{4}\left(\frac{1-\xi}{\xi(1+\xi)^2} - \frac{\arctan\sqrt{\xi}}{\xi^{3/2}}\right),$$

$$\mathcal{R}'_L(\xi) = \frac{(1+\xi)\arctan\sqrt{\xi}}{2\,\xi^{3/2}} + \frac{\xi-1}{2\xi\,(1+\xi)}\,.$$

Eqs. (25) together with (20) give us three coupled partial differential equations for the parameters $\xi(\tau,\varsigma)$, $\vartheta(\tau,\varsigma)$ and $p_{\rm hard}(\tau,\varsigma)$ of the RS ansatz (13). Their evolution will describe

[5] A similar structure of these equations was first found by Satarov et al. [29, 30].

the transition between early-time dynamics and late-time hydrodynamical behaviour for a non-boost-invariant plasma in a unified framework.

The (0+1)-dimensional boost invariant case can be recovered within our approach if we require that $\vartheta(\tau,\varsigma)=\varsigma$, $\xi(\tau,\varsigma)=\xi(\tau)$ and $p_{\rm hard}(\tau,\varsigma)=p_{\rm hard}(\tau)$. By taking this limit in Eqs. (20) and (25) and rearranging some terms, we obtain two differential equations for $\xi(\tau)$ and $p_{\rm hard}(\tau)$

$$\frac{1}{1+\xi}\partial_\tau\xi-\frac{2}{\tau}-\frac{6}{p_{\rm hard}}\partial_\tau p_{\rm hard}=2\Gamma\left[1-\mathcal{R}^{3/4}(\xi)\sqrt{1+\xi}\right]\,, \tag{26a}$$

$$\frac{\mathcal{R}'(\xi)}{\mathcal{R}(\xi)}\partial_\tau\xi+\frac{4}{p_{\rm hard}}\partial_\tau p_{\rm hard}=\frac{1}{\tau}\left[\frac{1}{\xi(1+\xi)\mathcal{R}(\xi)}-\frac{1}{\xi}-1\right]\,. \tag{26b}$$

The last expressions correspond precisely to the boost invariant case studied before by us (see Eqs. (20) and (22) in Ref. [13]). For the boost invariant case, one can also show that free streaming and ideal hydrodynamical behaviour are reproduced when $\Gamma=0$ and $\Gamma\to\infty$, respectively [13]. In addition, the (0+1)-dimensional 2nd-order viscous hydrodynamics of Israel and Stewart can be recovered from our ansatz in the small ξ limit if we identify [13][6]

$$\Gamma = \frac{2}{\tau_\pi}\,, \tag{27a}$$

$$\tau_\pi = \frac{5}{4}\frac{\eta}{\mathcal{P}}\,. \tag{27b}$$

We will implement this matching in our numerical simulations of the non-boost-invariant evolution equations (20) and (25). In this manner the evolution of the system is specified by the shear viscosity with no need to introduce additional parameters, e.g. thermalization time scales, etc.

3. Results and Discussion

In this section we present the results of numerically integrating the coupled nonlinear differential equations using the relation between the relaxation rate Γ and the ratio of shear viscosity to equilibrium entropy $\bar{\eta}\equiv\eta/\mathcal{S}$ which results from Eqs. (27), namely

$$\Gamma=\frac{2T(\tau)}{5\bar{\eta}}=\frac{2\mathcal{R}^{1/4}(\xi)p_{\rm hard}}{5\bar{\eta}}\,, \tag{28}$$

which should be used for Γ in Eqs. (20) and (25).

3.1. Initial Conditions

In order to minimize the number of figures presented here we will only consider LHC-like initial conditions. Additionally, for purposes of this paper we will present two types of initial

[6] We refer the reader to Sect. 2.4 of Ref. [13] for further details.

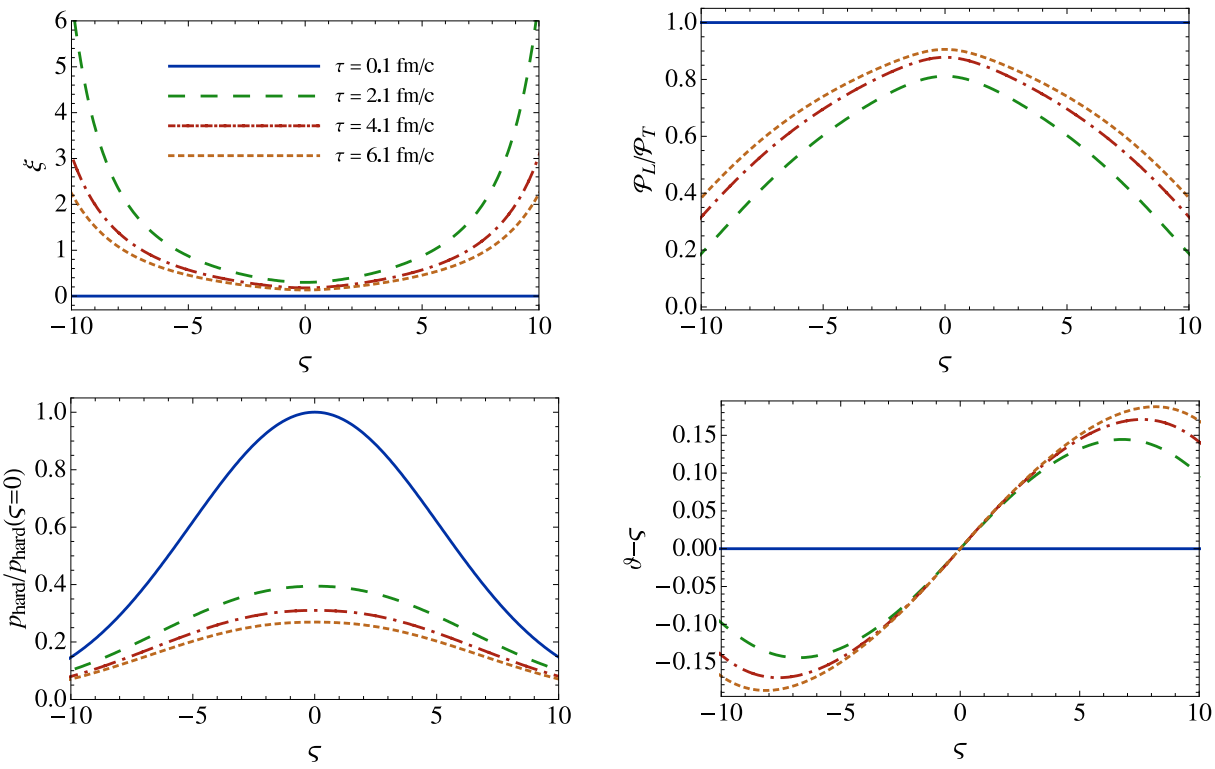

Figure 1: Evolution of the rapidity dependence of the dynamical variables in the case of isotropic Gaussian initial conditions and strong coupling viscosity corresponding to $\bar{\eta} = 1/(4\pi)$.

conditions: (I) an initially isotropic distribution which has a Gaussian profile in the number density and (II) an initially anisotropic distribution which has the same Gaussian density profile as case (I). For the number density profile in spatial rapidity (ς) we use a Gaussian which successfully describes experimentally observed pion rapidity spectra from AGS to RHIC energies [31–35] and extrapolate this result to LHC energies. The parametrization we use is

$$n(\varsigma) = n_0 \exp\left(-\frac{\varsigma^2}{2\sigma_\varsigma^2}\right) , \tag{29}$$

with

$$\sigma_\varsigma^2 = \frac{8}{3}\frac{c_s^2}{(1-c_s^4)} \ln\left(\sqrt{s_{NN}}/2m_p\right) , \tag{30}$$

where c_s is the sound velocity, $m_p = 0.938$ GeV is the proton mass, for LHC $\sqrt{s_{NN}} = 5.5$ TeV is the nucleon-nucleon center-of-mass energy, and n_0 is the number density at central rapidity. In this paper we will use an ideal equation of state for which $c_s = 1/\sqrt{3}$ in natural units.

In case (I) we can use Eq. (29) to straightforwardly calculate the initial dependence of $p_{\rm hard}$ on rapidity by using Eq. (A.2) with $\xi(\varsigma, \tau = \tau_0) = 0$ to obtain

$$p_{\rm hard}(\varsigma, \tau = 0) = p_0 \left[\exp\left(-\frac{\varsigma^2}{2\sigma_\varsigma^2}\right)\right]^{1/3} , \tag{31}$$

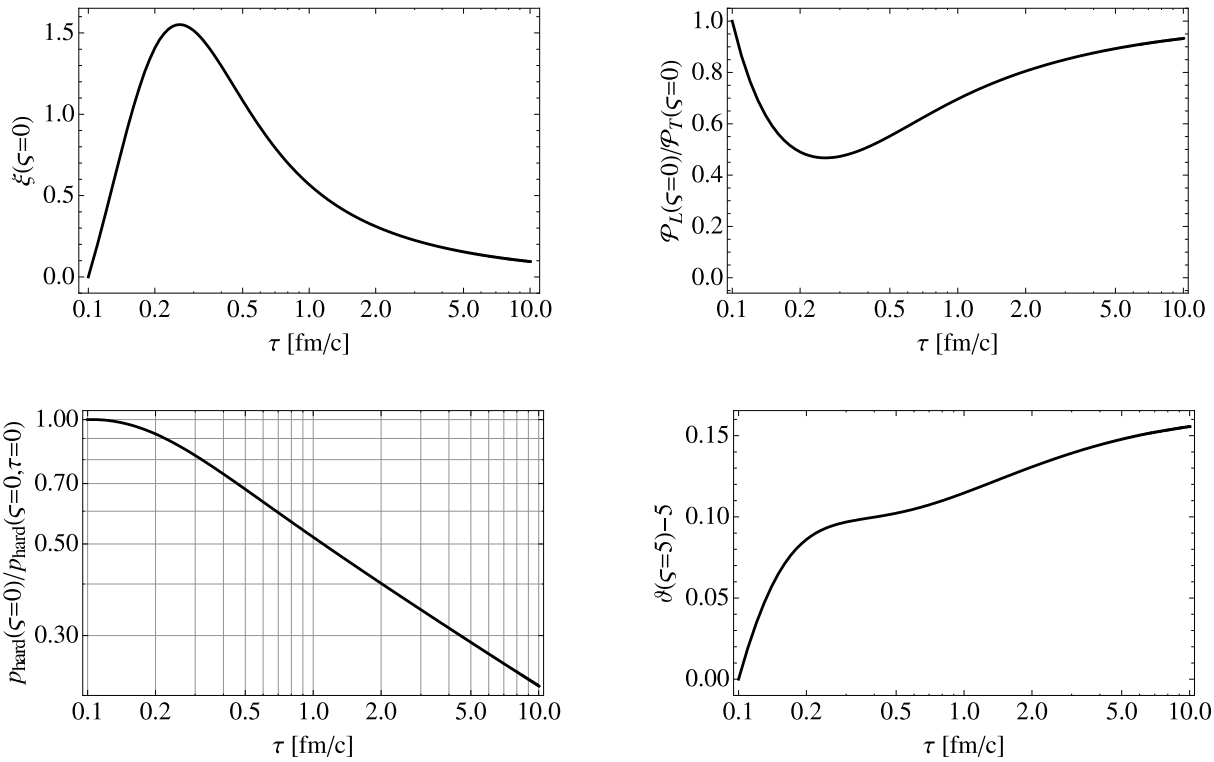

Figure 2: Evolution of the dynamical variables in the case of isotropic Gaussian initial conditions and strong coupling viscosity corresponding to $\bar{\eta} = 1/(4\pi)$. All panels show evolution at central rapidity, except panel showing time evolution of the hyperbolic angle $\theta - \varsigma$ which shows the evolution at $\varsigma = 5$.

where $p_0 = p_{\rm hard}(\varsigma = 0, \tau = 0)$ is the initial "temperature" at central rapidity. For LHC conditions we use $p_0 = 845$ MeV at an initial time of $\tau_0 = 0.1$ fm/c. In case (II) we choose $\xi(\varsigma, \tau = \tau_0) = 100$ which means that we should increase the central value of $p_{\rm hard}$ by a factor of $(1 + \xi)^{1/6} \simeq 2.16$ in order to start with the same initial particle density distribution [see Eq. (A.2)]. Doing this gives in case (II) $p_0 \simeq 1.82$ GeV.

In both cases (I) and (II) we must also fix the initial condition for the hyperbolic angle ϑ which specifies the four-velocity of the local rest frame. Here we choose $\vartheta(\varsigma, \tau = \tau_0) = \varsigma$ following Refs. [24, 29, 30]. This is not the most general initial condition possible, of course; however, absent some guiding principle we choose here to follow Refs. [24, 29, 30] and approximate the initial state as having a four-velocity profile corresponding to an initially boost-invariant configuration.

3.2. Case I: Isotropic Initial Conditions

In this subsection we present results for the spatial-rapidity and proper-time dependence of our dynamic parameters in the case that the parton distribution function is assumed to be locally isotropic at $\tau = \tau_0 = 0.1$ fm/c. We present the cases of transport coefficients corresponding to a strongly-coupled plasma and a weakly-coupled plasma separately.

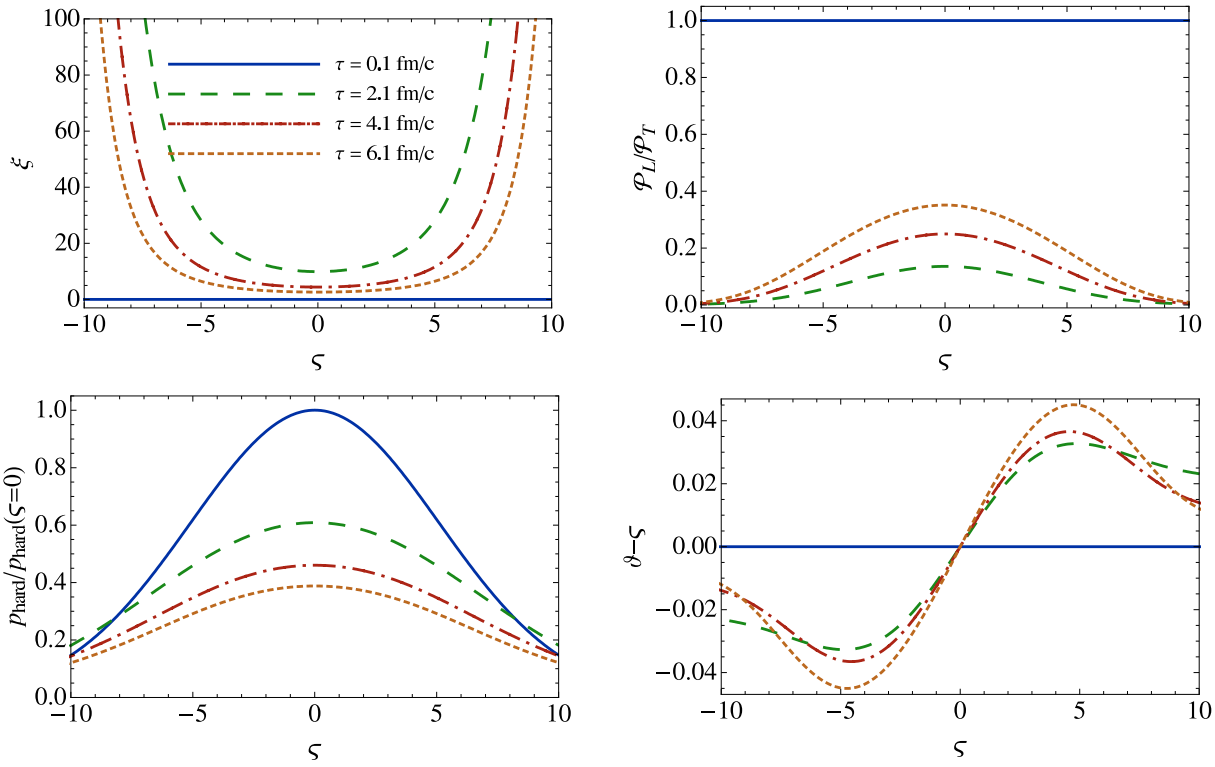

Figure 3: Evolution of the rapidity dependence of the dynamical variables in the case of isotropic Gaussian initial conditions and weak coupling viscosity corresponding to $\bar{\eta} = 10/(4\pi)$.

3.2.1. Strongly Coupled

In Fig. 1 we plot the spatial-rapidity dependence of the anisotropy parameter (upper left), the ratio of the longitudinal to transverse pressure (upper right), the hard momentum scale (lower left), and the hyperbolic angle of the local rest frame four-velocity as measured in the lab frame (lower right). We have fixed the ratio of the shear viscosity to entropy density to be $\bar{\eta} \equiv \eta/\mathcal{S} = 1/(4\pi)$. Each line in the plot corresponds to a fixed proper-time $\tau \in \{0.1, 2.1, 4.1, 6.1\}$ fm/c. From these figures we see that large momentum-space anisotropies are developed at large rapidity. This can be traced back to the fact that the initial temperature is lower at large rapidity, causing the rate of relaxation back to isotropy to be slower [9]. At $\tau = 6.1$ fm/c we see that in the case of strong-coupling shear viscosity at $\varsigma = 5$, $\mathcal{P}_L/\mathcal{P}_T \simeq 0.75$.

We note that the deviation of $\vartheta \neq \varsigma$ which results for $\tau > \tau_0$ is indicative of the breaking of longitudinal boost invariance. The fact that $\vartheta > \varsigma$ results from there being pressure gradients in the longitudinal direction which increase the longitudinal velocity beyond that which would be obtained if the flow were boost invariant. The fact that the $\vartheta - \varsigma$ curves turn over at large spatial rapidity is an indication that the material at the edges is propagating at a slower longitudinal velocity than the material in the central region. We also note that as shown in the lower left plot of the hard momentum scale both the width and amplitude of the momentum distribution are changing with proper-time. The is width increasing with

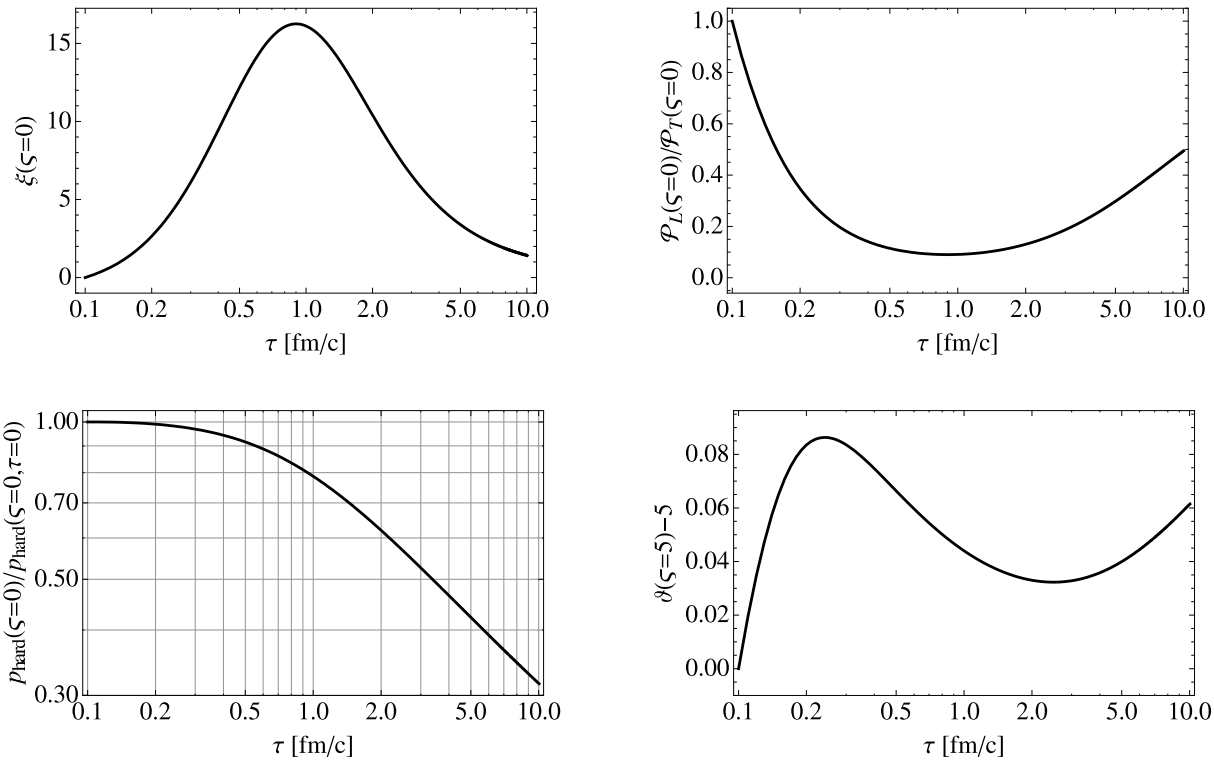

Figure 4: Evolution of the dynamical variables in the case of isotropic Gaussian initial conditions and weak coupling viscosity corresponding to $\bar{\eta} = 10/(4\pi)$. All panels show evolution at central rapidity, except panel showing time evolution of the hyperbolic angle $\theta - \varsigma$ which shows the evolution at $\varsigma = 5$.

proper-time due to longitudinal pressure gradients.

In Fig. 2 we plot the proper-time dependence of our dynamical variables and the pressure anisotropy for fixed spatial rapidity. We show the anisotropy parameter at central rapidity (upper left), the ratio of the longitudinal to transverse pressure at central rapidity (upper right), the hard momentum scale at central rapidity (lower left), and the hyperbolic angle of the local rest frame four-velocity as measured in the lab frame at $\varsigma = 5$ (lower right). We do not show ϑ at central rapidity since $\vartheta(\varsigma = 0) = 0$ by symmetry [29, 30]. As one can see from the plots presented in Fig. 2 at central rapidities large momentum-space anisotropies can develop at early times even in the case of a strongly-coupled plasma. From the upper right panel of Fig. 2 we see that at $\tau \simeq 0.25$ fm/c one has $\mathcal{P}_L/\mathcal{P}_T \lesssim 0.5$. Such large pressure anisotropies could have a significant effect on observables which are sensitive to the early-time dynamics of the quark-gluon plasma such as photon [36–42], dilepton [25, 26, 43, 44] and heavy-quarkonium production [45–54].

3.2.2. Weakly Coupled

In Fig. 3 we plot the spatial-rapidity dependence of the anisotropy parameter (upper left), the ratio of the longitudinal to transverse pressure (upper right), the hard momentum scale (lower left), and the hyperbolic angle of the local rest frame four-velocity as measured in the lab frame (lower right). We have fixed the ratio of the shear viscosity to entropy

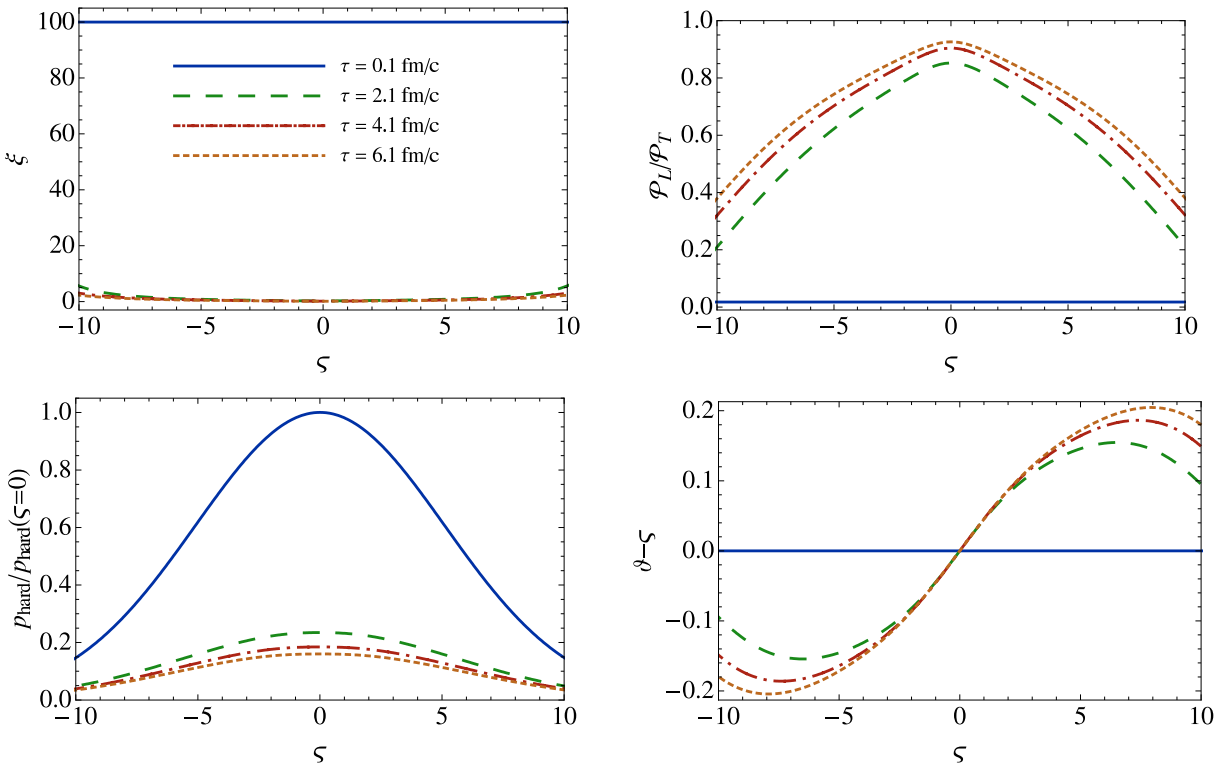

Figure 5: Evolution of the rapidity dependence of the dynamical variables in the case of anisotropic Gaussian initial conditions and strong coupling viscosity corresponding to $\bar{\eta} = 1/(4\pi)$. Initial value of ξ is $\xi_0 = 100$, independent of rapidity.

density to be $\bar{\eta} \equiv \eta/\mathcal{S} = 10/(4\pi)$. Each line in the plot corresponds to a fixed proper-time $\tau \in \{0.1, 2.1, 4.1, 6.1\}$ fm/c. From these figures we see that large momentum-space anisotropies are developed at all rapidities. At $\tau = 6.1$ fm/c we see that in the case of weak-coupling shear viscosity $\mathcal{P}_L/\mathcal{P}_T \lesssim 0.4$ at all rapidities. In terms of the hyperbolic angle ϑ we see weaker deviations from boost-invariant longitudinal flow than seen in the case of strong-coupling transport coefficients (Fig. 1). Such strong momentum-space anisotropies indicate that a naive viscous hydrodynamical treatment would not be trustworthy at any spatial rapidity shown. This is in line with the results presented in Ref. [9] where we discussed the generation of negative longitudinal pressure due to large momentum-space anisotropies when using 2nd-order viscous hydrodynamical evolution equations. Using the partial-differential equations presented here we are able to evolve the system even in the case of large momentum-space anisotropies and the longitudinal pressure is guaranteed to be positive at all times.

In Fig. 4 we plot the proper-time dependence of our dynamical variables and the pressure anisotropy for fixed spatial rapidity. We show the anisotropy parameter at central rapidity (upper left), the ratio of the longitudinal to transverse pressure at central rapidity (upper right), the hard momentum scale at central rapidity (lower left), and the hyperbolic angle of the local rest frame four-velocity as measured in the lab frame at $\varsigma = 5$ (lower right). As one can see from the plots presented in Fig. 4 at central rapidities large momentum-

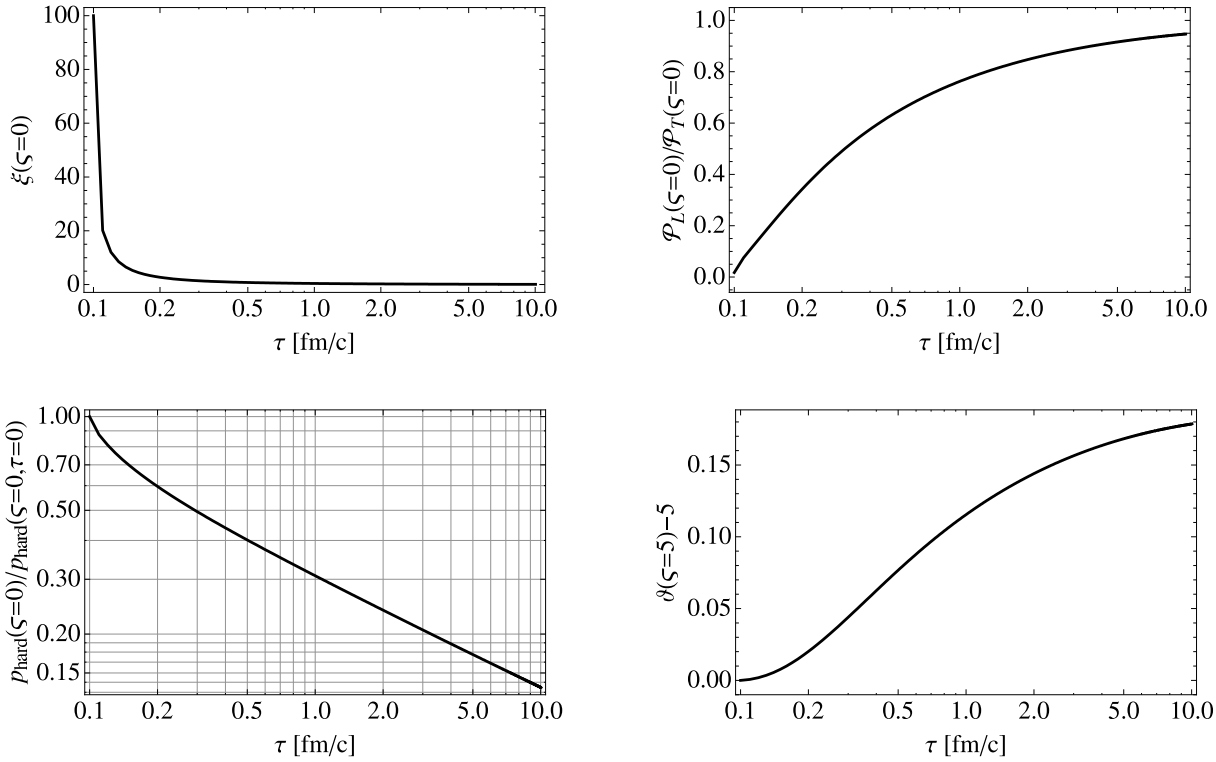

Figure 6: Evolution of the dynamical variables in the case of anisotropic Gaussian initial conditions and strong coupling viscosity corresponding to $\bar{\eta} = 1/(4\pi)$. All panels show evolution at central rapidity, except panel showing time evolution of the hyperbolic angle $\theta - \varsigma$ which shows the evolution at $\varsigma = 5$. Initial value of ξ is $\xi_0 = 100$, independent of rapidity.

space anisotropies persist at all times. From the upper right panel of Fig. 4 we see that at $\tau \simeq 0.25$ fm/c one has $\mathcal{P}_L/\mathcal{P}_T \lesssim 0.25$. This is much larger than the strongly-coupled case presented in the previous section. This suggests that anisotropic photon, dilepton, and heavy-quarkonium production rates integrated in spacetime using our dynamical model could be used to constrain quark-gluon transport coefficients. This could be done by comparing theoretical predictions resulting from the assumption of strong-coupling (Fig. 1) and weak-coupling (Fig. 3) transport coefficients and integrating over the resulting spacetime evolution. Finally we point out that one sees from the lower left panel of Fig. 4 that the evolution of the hard momentum scale is far from that expected due to weakly-viscous expansion. Initially we see a period of approximate free-streaming expansion which later transitions to viscous hydrodynamical expansion. This would have the effect of increasing the lifetime of the quark-gluon plasma in the weakly-coupled case and could result in stronger transverse flow than naively predicted by a 2nd-order viscous hydrodynamical treatment.

3.3. Case II: Anisotropic Initial Conditions

In this subsection we present results for the spatial-rapidity and proper-time dependence of our dynamical parameters in the case that the parton distribution function is assumed to be locally anisotropic at $\tau = \tau_0 = 0.1$ fm/c. As detailed in the beginning of the results

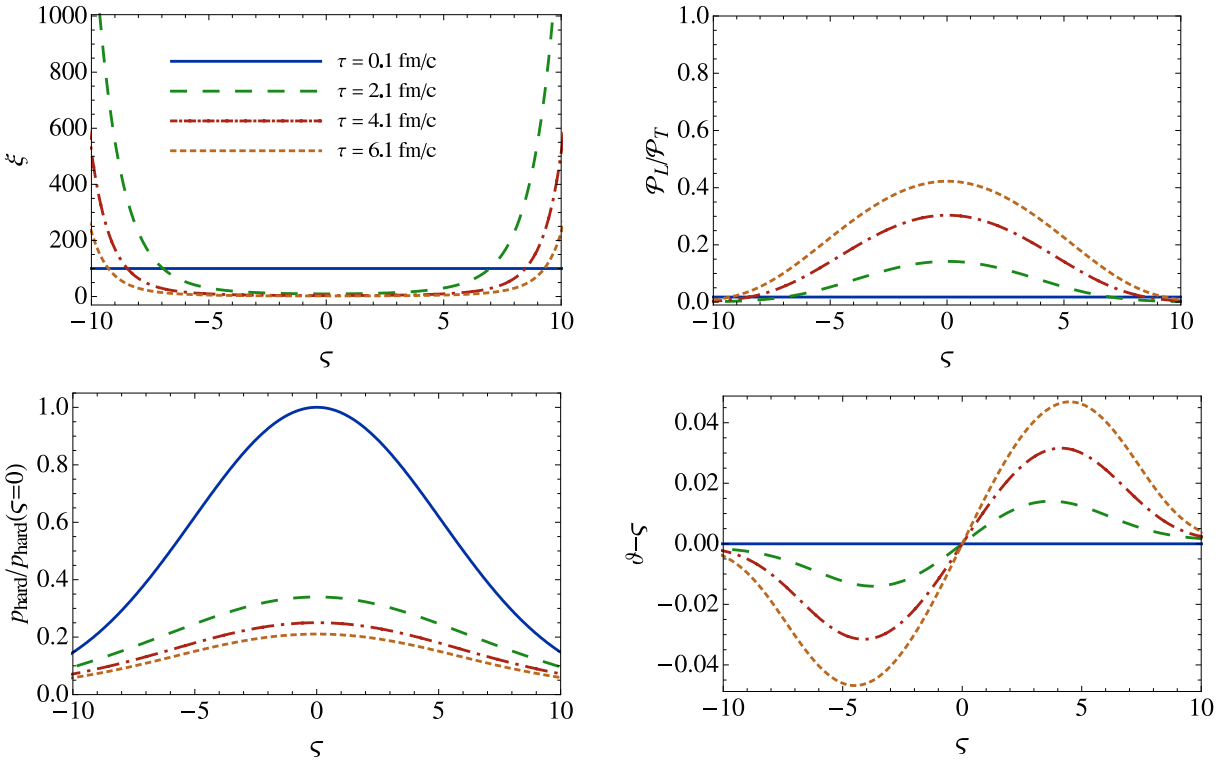

Figure 7: Evolution of the rapidity dependence of the dynamical variables in the case of anisotropic Gaussian initial conditions and weak coupling viscosity corresponding to $\bar{\eta} = 10/(4\pi)$. Initial value of ξ is $\xi_0 = 100$, independent of rapidity.

section we take $\xi(\tau_0) = 100$ which corresponds to a highly oblate distribution with $\mathcal{P}_L \ll \mathcal{P}_T$. Such highly oblate distributions are predicted by color-glass-condensate models of the early-time dynamics of a heavy-ion collision [19, 55]. As in the previous section that assumed isotropic initial conditions, we present the cases of transport coefficients corresponding to a strongly-coupled plasma and a weakly-coupled plasma separately.

3.3.1. Strongly Coupled

In Fig. 5 we plot the spatial-rapidity dependence of the anisotropy parameter (upper left), the ratio of the longitudinal to transverse pressure (upper right), the hard momentum scale (lower left), and the hyperbolic angle of the local rest frame four-velocity as measured in the lab frame (lower right). We have fixed the ratio of the shear viscosity to entropy density to be $\bar{\eta} \equiv \eta/\mathcal{S} = 1/(4\pi)$. Each line in the plot corresponds to a fixed proper-time $\tau \in \{0.1, 2.1, 4.1, 6.1\}$ fm/c. From these figures we see that large momentum-space anisotropies persist at large rapidity. At $\tau = 6.1$ fm/c we see that in the case of strong-coupling shear viscosity at $\varsigma = 5$, $\mathcal{P}_L/\mathcal{P}_T \simeq 0.7$. This is similar in magnitude to the result obtained when one starts with an isotropic initial condition (see Fig. 1). We also note a characteristic triangular shape to the spatial-rapidity dependence of the pressure anisotropy (Fig. 5 top right).

In Fig. 6 we plot the proper-time dependence of our dynamical variables and the pressure

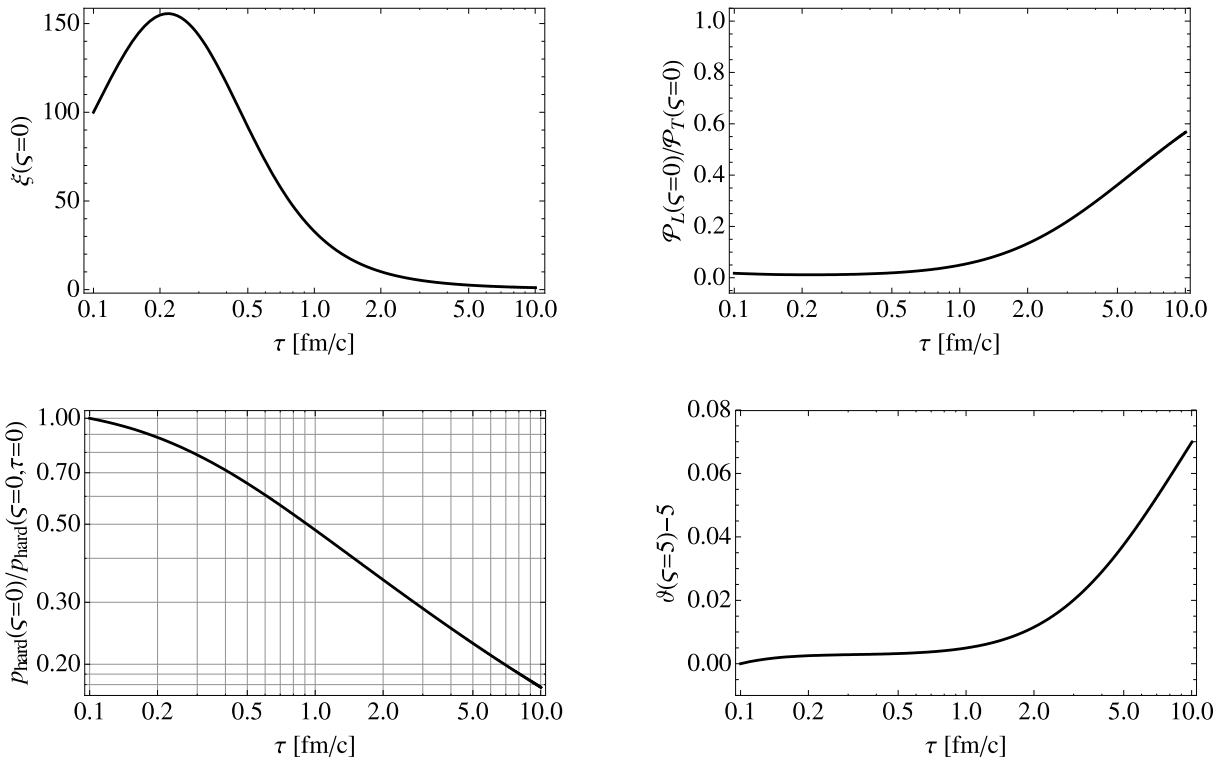

Figure 8: Evolution of the dynamical variables in the case of anisotropic Gaussian initial conditions and weak coupling viscosity corresponding to $\bar{\eta} = 10/(4\pi)$. All panels show evolution at central rapidity, except panel showing time evolution of the hyperbolic angle $\theta - \varsigma$ which shows the evolution at $\varsigma = 5$. Initial value of ξ is $\xi_0 = 100$, independent of rapidity.

anisotropy for fixed spatial-rapidity. We show the anisotropy parameter at central rapidity (upper left), the ratio of the longitudinal to transverse pressure at central rapidity (upper right), the hard momentum scale at central rapidity (lower left), and the hyperbolic angle of the local rest frame four-velocity as measured in the lab frame at $\varsigma =$ (lower right). As one can see from the plots presented in Fig. 6 at central rapidities large momentum-space anisotropies persist in the case of a strongly-coupled plasma. From the upper right panel of Fig. 6 we see that at $\tau \simeq 0.25$ fm/c one has $\mathcal{P}_L/\mathcal{P}_T \lesssim 0.5$. This is similar to the case of isotropic initial conditions suggesting a kind of "attractor" for the momentum-space anisotropy evolution. This attractor can be identified as the Navier-Stokes solution if one analyzes the late time asymptotic solutions of the evolution equations presented here and/or 2nd-order viscous hydrodynamics.

3.3.2. Weakly Coupled

In Fig. 7 we plot the spatial-rapidity dependence of the anisotropy parameter (upper left), the ratio of the longitudinal to transverse pressure (upper right), the hard momentum scale (lower left), and the hyperbolic angle of the local rest frame four-velocity as measured in the lab frame (lower right). We have fixed the ratio of the shear viscosity to entropy density to be $\bar{\eta} \equiv \eta/\mathcal{S} = 10/(4\pi)$. Each line in the plot corresponds to a fixed proper-

time $\tau \in \{0.1, 2.1, 4.1, 6.1\}$ fm/c. From these figures we see that large momentum-space anisotropies are developed at all rapidities. At $\tau = 6.1$ fm/c we see that in the case of weak-coupling shear viscosity at $\varsigma = 5$, $\mathcal{P}_L/\mathcal{P}_T \simeq 0.2$.

In Fig. 8 we plot the proper-time dependence of our dynamical variables and the pressure anisotropy for fixed spatial rapidity. We show the anisotropy parameter at central rapidity (upper left), the ratio of the longitudinal to transverse pressure at central rapidity (upper right), the hard momentum scale at central rapidity (lower left), and the hyperbolic angle of the local rest frame four-velocity as measured in the lab frame at $\varsigma =$ (lower right). As one can see from the plots presented in Fig. 8 at central rapidities large momentum-space anisotropies persist for a long time in the case of an initially anisotropic weakly-coupled quark-gluon plasma. From the upper right panel of Fig. 8 we see that at $\tau \simeq 0.25$ fm/c one has $\mathcal{P}_L/\mathcal{P}_T \lesssim 0.01$. Such extreme momentum-space anisotropies would preclude the use of a viscous hydrodynamical treatment; however, our reorganized expansion offers some hope to treat systems with such high anisotropies.

4. Conclusions and Outlook

In this paper we have derived three coupled partial differential equations given in Eqs. (20) and (25) whose solution gives the time evolution of the plasma anisotropy parameter ξ, the typical hard momentum scale of the partons $p_{\rm hard}$, and the longitudinal flow velocity variable ϑ. We relaxed the assumption of boost-invariance by allowing the longitudinal flow velocity variable to differ from the spatial rapidity ς and we also allowed the hard momentum scale and plasma anisotropy to depend on the spatial rapidity. The partial differential equations were obtained by taking moments of the Boltzmann equation using a relaxation time approximation collisional kernel and a spheroidally anisotropic ansatz for the underlying partonic distribution function. By requiring that our equations reduced to 2nd order viscous hydrodynamics in the limit of small anisotropy we were able to obtain an analytic connection between the relaxation rate Γ appearing in the collisional kernel and the plasma shear viscosity η and shear relaxation time τ_π. Using Eqs. (20) and (25) and Γ as a functions of η we were able to numerically solve the coupled partial differential equations in both the strong and weak coupling limits.

Our numerical results indicate that in both the strongly and weakly coupled cases large momentum-space anisotropies can be generated. Therefore, a treatment such as the one derived here in which momentum-space anisotropies are built into the leading order ansatz can better describe the time evolution of the system. Relatedly we demonstrated that within our reorganized approach at all spatial rapidity the longitudinal pressure remains positive during the entire evolution. This is to be contrasted to 2nd-order viscous hydrodynamics which can give negative pressures indicating the breakdown of the expansion about an isotropic equilibrium state. We have also discussed the fact that our equations can reproduce both extreme limits of the dynamics: ideal hydrodynamical expansion when the shear viscosity goes to zero and free streaming when the shear viscosity goes to infinity.

The numerical results obtained here differ from those obtained in Ref. [24] in that we see a much slower relaxation to isotropy at large spatial rapidity. This results from the fact that

the authors of Ref. [24] assumed that there is a single rapidity-independent thermalization time scale which they arbitrarily chose to be 0.25 fm/c. In this work we instead implemented a method for matching to 2nd-order viscous hydrodynamics that was introduced by us in Ref. [13]. The conclusion of that paper was that the relaxation rate Γ should be proportional to hard momentum scale (see Eq. (28) herein). If in a certain region the average momentum scale is lower, as is the case in the forward regions described by large spatial rapidity, this implies a slower relaxation to isotropic equilibrium. In our case this naturally arises due to the matching to 2nd-order viscous hydrodynamics in the limit of small anisotropy and as a result it not necessary to introduce external parameters such as thermalization times as a function of rapidity.

Beside the interesting theoretical goal of improving the description of systems which have large momentum-space anisotropies, we point out that the dynamical equations derived here can be used to assess the impact of rapidity-dependent moment-space anisotropies on observables which are sensitive to the early-time dynamics of the quark-gluon plasma such as photon [36–42], dilepton [25, 26, 43, 44] and heavy-quarkonium production [45–54]. Additionally, one could consider using the evolution of ξ and $p_{\rm hard}$ presented here in order to fold in a realistic anisotropy evolution into simulations of non-abelian plasma instabilities [10, 56–63].

Looking forward it is of critical importance to include the transverse expansion and elliptical flow of the system. This can be done minimally by allowing for one more momentum-space anisotropy parameter that describes the momentum-space anisotropy in the transverse plane and allowing all dynamical parameters to depend on proper-time, spatial rapidity, and transverse position. Work along these lines is currently underway [14].

Acknowledgments

We thank G. Denicol and I. Mishustin for useful discussions. We thank D. Bazow for checking our numerical results. M. Martinez and M. Strickland were supported by the Helmholtz International Center for FAIR Landesoffensive zur Entwicklung Wissenschaftlich-Ökonomischer Exzellenz program.

Appendix A. Analytic expressions for the components of the energy momentum tensor, number density, and entropy density

The energy-momentum tensor $T^{\mu\nu} = (2\pi)^{-3} \int d^3\mathbf{p}/p^0\, p^\mu p^\nu f(x,p,t)$ for the RS ansatz (13) is diagonal in the comoving frame and its components are [13, 28]

$$\mathcal{E}(p_{\rm hard},\xi) = T^{\tau\tau} = \frac{1}{2}\left(\frac{1}{1+\xi} + \frac{\arctan\sqrt{\xi}}{\sqrt{\xi}}\right)\mathcal{E}_{\rm iso}(p_{\rm hard})\,, \tag{A.1a}$$

$$\equiv \mathcal{R}(\xi)\,\mathcal{E}_{\rm iso}(p_{\rm hard})\,,$$

$$\mathcal{P}_T(p_{\rm hard},\xi) = \frac{1}{2}\left(T^{xx}+T^{yy}\right) = \frac{3}{2\xi}\left(\frac{1+(\xi^2-1)\mathcal{R}(\xi)}{\xi+1}\right)\mathcal{P}_T^{\rm iso}(p_{\rm hard})\,, \tag{A.1b}$$

$$\equiv \mathcal{R}_{\rm T}(\xi)\mathcal{P}_T^{\rm iso}(p_{\rm hard})\,,$$

$$\mathcal{P}_L(p_{\rm hard},\xi) = -T^{\varsigma}_{\varsigma} = \frac{3}{\xi}\left(\frac{(\xi+1)\mathcal{R}(\xi)-1}{\xi+1}\right)\mathcal{P}_L^{\rm iso}(p_{\rm hard})\,, \tag{A.1c}$$

$$\equiv \mathcal{R}_{\rm L}(\xi)\mathcal{P}_L^{\rm iso}(p_{\rm hard})\,,$$

where $\mathcal{P}_T^{\rm iso}(p_{\rm hard})$ and $\mathcal{P}_L^{\rm iso}(p_{\rm hard})$ are the isotropic transverse and longitudinal pressures and $\mathcal{E}_{\rm iso}(p_{\rm hard})$ is the isotropic energy density.

One can also easily obtain the number density as a function of $p_{\rm hard}$ and ξ

$$n(\xi,p_{\rm hard}) = \frac{n_{\rm iso}(p_{\rm hard})}{\sqrt{1+\xi}} \propto \frac{p_{\rm hard}^3}{\sqrt{1+\xi}}\,, \tag{A.2}$$

where $n_{\rm iso}$ is the isotropic number density. Similarly, one can obtain for the entropy density

$$\mathcal{S}(\xi,p_{\rm hard}) = \frac{\mathcal{S}_{\rm iso}(p_{\rm hard})}{\sqrt{1+\xi}}\,. \tag{A.3}$$

References

[1] P. Huovinen, P. F. Kolb, U. W. Heinz, P. V. Ruuskanen, and S. A. Voloshin, "Radial and elliptic flow at RHIC: further predictions," *Phys. Lett.* **B503** (2001) 58–64, arXiv:hep-ph/0101136.

[2] T. Hirano and K. Tsuda, "Collective flow and two pion correlations from a relativistic hydrodynamic model with early chemical freeze out," *Phys. Rev.* **C66** (2002) 054905, arXiv:nucl-th/0205043.

[3] M. J. Tannenbaum, "Recent results in relativistic heavy ion collisions: From 'a new state of matter' to 'the perfect fluid'," *Rept. Prog. Phys.* **69** (2006) 2005–2060, arXiv:nucl-ex/0603003.

[4] P. F. Kolb and U. W. Heinz, "Hydrodynamic description of ultrarelativistic heavy-ion collisions," arXiv:nucl-th/0305084.

[5] K. Dusling and D. Teaney, "Simulating elliptic flow with viscous hydrodynamics," *Phys. Rev.* **C77** (2008) 034905, arXiv:0710.5932 [nucl-th].

[6] M. Luzum and P. Romatschke, "Conformal Relativistic Viscous Hydrodynamics: Applications to RHIC results at sqrt(sNN) = 200 GeV," *Phys. Rev.* **C78** (2008) 034915, arXiv:0804.4015 [nucl-th].

[7] H. Song and U. W. Heinz, "Extracting the QGP viscosity from RHIC data – a status report from viscous hydrodynamics," arXiv:0812.4274 [nucl-th].

[8] U. W. Heinz, "Early collective expansion: Relativistic hydrodynamics and the transport properties of QCD matter," arXiv:0901.4355 [nucl-th].

[9] M. Martinez and M. Strickland, "Constraining relativistic viscous hydrodynamical evolution," *Phys. Rev.* **C79** (2009) 044903, arXiv:0902.3834 [hep-ph].
[10] P. Romatschke and M. Strickland, "Collective Modes of an Anisotropic Quark-Gluon Plasma," *Phys. Rev.* **D68** (2003) 036004.
[11] M. Kröger, *Models for Polymeric and Anisotropic Liquids*. Springer, 2005.
[12] M. Abramowitz and I. A. Stegun, "Spheroidal wave functions," in *Handbook of Mathematical Functions with Formulas, Graphs, and Mathematical Tables*, pp. 751–770. Dover, New York, 1964.
[13] M. Martinez and M. Strickland, "Dissipative Dynamics of Highly Anisotropic Systems," *Nucl. Phys.* **A848** (2010) 183–197, arXiv:1007.0889 [nucl-th].
[14] M. Martinez and M. Strickland, forthcoming.
[15] S. R. de Groot, W. A. van Leewen, and C. G. van Weert, *Relativistic Kinetic Theory: principles and applications*. Elsevier North-Holland, 1980.
[16] W. Israel and J. M. Stewart, "Transient relativistic thermodynamics and kinetic theory," *Ann. Phys.* **118** (1979) 341–372.
[17] A. Muronga, "Relativistic Dynamics of Non-ideal Fluids: Viscous and heat-conducting fluids II. Transport properties and microscopic description of relativistic nuclear matter," *Phys. Rev.* **C76** (2007) 014910, arXiv:nucl-th/0611091.
[18] T. Biro, E. van Doorn, B. Muller, M. Thoma, and X. Wang, "Parton equilibration in relativistic heavy ion collisions," *Phys.Rev.* **C48** (1993) 1275–1284, arXiv:nucl-th/9303004 [nucl-th].
[19] R. Baier, A. H. Mueller, D. Schiff, and D. Son, "'Bottom up' thermalization in heavy ion collisions," *Phys.Lett.* **B502** (2001) 51–58, arXiv:hep-ph/0009237 [hep-ph].
[20] Z. Xu and C. Greiner, "Transport rates and momentum isotropization of gluon matter in ultrarelativistic heavy-ion collisions," *Phys.Rev.* **C76** (2007) 024911, arXiv:hep-ph/0703233 [hep-ph].
[21] Z. Xu and C. Greiner, "Thermalization of gluons in ultrarelativistic heavy ion collisions by including three-body interactions in a parton cascade," *Phys.Rev.* **C71** (2005) 064901, arXiv:hep-ph/0406278 [hep-ph].
[22] P. Romatschke, "New Developments in Relativistic Viscous Hydrodynamics," *Int.J.Mod.Phys.* **E19** (2010) 1–53, arXiv:arXiv:0902.3663 [hep-ph].
[23] W. Florkowski and R. Ryblewski, "Highly-anisotropic and strongly-dissipative hydrodynamics for early stages of relativistic heavy-ion collisions," arXiv:1007.0130 [nucl-th].
[24] R. Ryblewski and W. Florkowski, "Non-boost-invariant motion of dissipative and highly eq:gammamatcic fluid," arXiv:1007.4662 [nucl-th].
[25] M. Martinez and M. Strickland, "Measuring QGP thermalization time with dileptons," *Phys.Rev.Lett.* **100** (2008) 102301, arXiv:0709.3576 [hep-ph].
[26] M. Martinez and M. Strickland, "Pre-equilibrium dilepton production from an anisotropic quark-gluon plasma," *Phys.Rev.* **C78** (2008) 034917, arXiv:0805.4552 [hep-ph].
[27] G. Baym, "Thermal equilibration in Ultrarelativistic Heavy Ion Collisions," *Phys. Lett.* **B138** (1984) 18–22.
[28] M. Martinez and M. Strickland, "Matching pre-equilibrium dynamics and viscous hydrodynamics," *Phys. Rev.* **C81** (2010) 024906.
[29] L. Satarov, I. Mishustin, A. Merdeev, and H. Stoecker, "1+1 Dimensional Hydrodynamics for High-energy Heavy-ion Collisions," *Phys.Atom.Nucl.* **70** (2007) 1773–1796, arXiv:hep-ph/0611099 [hep-ph].
[30] L. Satarov, A. Merdeev, I. Mishustin, and H. Stoecker, "Longitudinal fluid-dynamics for ultrarelativistic heavy-ion collisions," *Phys.Rev.* **C75** (2007) 024903, arXiv:hep-ph/0606074 [hep-ph].
[31] **BRAHMS Collaboration** Collaboration, I. Bearden *et al.*, "Charged meson rapidity distributions in central Au+Au collisions at s(NN)**(1/2) = 200-GeV," *Phys.Rev.Lett.* **94** (2005) 162301, arXiv:nucl-ex/0403050 [nucl-ex].
[32] **PHOBOS** Collaboration, I. C. Park *et al.*, "Charged particle flow measurement for —eta— ¡ 5.3 with the PHOBOS detector," *Nucl. Phys.* **A698** (2002) 564–567, arXiv:nucl-ex/0105015.
[33] **PHOBOS Collaboration** Collaboration, B. Back *et al.*, "Charged-particle pseudorapidity

distributions in Au+Au collisions at s(NN)**1/2 = 62.4-GeV," *Phys.Rev.* **C74** (2006) 021901, arXiv:nucl-ex/0509034 [nucl-ex].
[34] **PHOBOS Collaboration** Collaboration, G. I. Veres *et al.*, "System size, energy, centrality and pseudorapidity dependence of charged-particle density in Au+Au and Cu+Cu collisions at RHIC," arXiv:arXiv:0806.2803 [nucl-ex].
[35] M. Bleicher, "Evidence for the onset of deconfinement from longitudinal momentum distributions? Observation of the softest point of the equation of state," arXiv:hep-ph/0509314 [hep-ph].
[36] B. Schenke and M. Strickland, "Photon production from an anisotropic quark-gluon plasma," *Phys. Rev.* **D76** (2007) 025023, arXiv:hep-ph/0611332.
[37] A. Ipp, A. Di Piazza, J. Evers, and C. H. Keitel, "Photon polarization as a probe for quark-gluon plasma dynamics," *Phys.Lett.* **B666** (2008) 315–319, arXiv:0710.5700 [hep-ph].
[38] L. Bhattacharya and P. Roy, "Measuring isotropization time of Quark-Gluon-Plasma from direct photon at RHIC," *Phys.Rev.* **C79** (2009) 054910, arXiv:0812.1478 [hep-ph].
[39] K. Dusling, "Photons as a viscometer of heavy ion collisions," *Nucl.Phys.* **A839** (2010) 70–77, arXiv:0903.1764 [nucl-th].
[40] A. Ipp, C. H. Keitel, and J. Evers, "Yoctosecond photon pulses from quark-gluon plasmas," *Phys.Rev.Lett.* **103** (2009) 152301, arXiv:0904.4503 [hep-ph].
[41] L. Bhattacharya and P. Roy, "Rapidity distribution of photons from an anisotropic Quark-Gluon-Plasma," *Phys.Rev.* **C81** (2010) 054904, arXiv:0907.3607 [hep-ph].
[42] L. Bhattacharya and P. Roy, "Jet-photons from an anisotropic *Quark-Gluon-Plasma*," *J.Phys.G* **G37** (2010) 105010, arXiv:1001.1054 [hep-ph].
[43] M. Martinez and M. Strickland, "Suppression of forward dilepton production from an anisotropic quark-gluon plasma," *Eur.Phys.J.* **C61** (2009) 905–913, arXiv:0808.3969 [hep-ph].
[44] K. Dusling and S. Lin, "Dilepton production from a viscous QGP," *Nucl.Phys.* **A809** (2008) 246–258, arXiv:0803.1262 [nucl-th].
[45] A. Dumitru, Y. Guo, and M. Strickland, "The Heavy-quark potential in an anisotropic (viscous) plasma," *Phys.Lett.* **B662** (2008) 37–42, arXiv:0711.4722 [hep-ph].
[46] A. Dumitru, Y. Guo, A. Mocsy, and M. Strickland, "Quarkonium states in an anisotropic QCD plasma," *Phys.Rev.* **D79** (2009) 054019, arXiv:0901.1998 [hep-ph].
[47] A. Dumitru, Y. Guo, and M. Strickland, "The Imaginary part of the static gluon propagator in an anisotropic (viscous) QCD plasma," *Phys.Rev.* **D79** (2009) 114003, arXiv:0903.4703 [hep-ph].
[48] R. Baier and Y. Mehtar-Tani, "Jet quenching and broadening: The Transport coefficient q-hat in an anisotropic plasma," *Phys.Rev.* **C78** (2008) 064906, arXiv:0806.0954 [hep-ph].
[49] J. Noronha and A. Dumitru, "The Heavy Quark Potential as a Function of Shear Viscosity at Strong Coupling," *Phys.Rev.* **D80** (2009) 014007, arXiv:0903.2804 [hep-ph].
[50] Y. Burnier, M. Laine, and M. Vepsalainen, "Quarkonium dissociation in the presence of a small momentum space anisotropy," *Phys.Lett.* **B678** (2009) 86–89, arXiv:0903.3467 [hep-ph].
[51] M. Carrington and A. Rebhan, "On the imaginary part of the next-to-leading-order static gluon self-energy in an anisotropic plasma," *Phys.Rev.* **80** (2009) 065035, arXiv:0906.5220 [hep-ph].
[52] O. Philipsen and M. Tassler, "On Quarkonium in an anisotropic quark gluon plasma," arXiv:0908.1746 [hep-ph].
[53] V. Chandra and V. Ravishankar, "Quarkonia in anisotropic hot QCD medium in a quasi-particle model," *Nucl. Phys A (2010)* (2010) , arXiv:1006.3995 [nucl-th].
[54] P. Roy and A. K. Dutt-Mazumder, "Radiative energy loss in an anisotropic Quark-Gluon-Plasma," arXiv:1009.2304 [nucl-th]. * Temporary entry *.
[55] F. Gelis, E. Iancu, J. Jalilian-Marian, and R. Venugopalan, "The Color Glass Condensate," arXiv:1002.0333 [hep-ph]. * Temporary entry *.
[56] "Plasma instability at the initial stage of ultrarelativistic heavy-ion collisions," *Physics Letters B* **314** no. 1, (1993) 118 – 121.
[57] P. B. Arnold, J. Lenaghan, and G. D. Moore, "QCD plasma instabilities and bottom up thermalization," *JHEP* **0308** (2003) 002, arXiv:hep-ph/0307325 [hep-ph]. Erratum added online,

sep/29/2004.

[58] A. Rebhan, P. Romatschke, and M. Strickland, "Hard-loop dynamics of non-Abelian plasma instabilities," *Phys.Rev.Lett.* **94** (2005) 102303, arXiv:hep-ph/0412016 [hep-ph].

[59] P. B. Arnold, G. D. Moore, and L. G. Yaffe, "The Fate of non-Abelian plasma instabilities in 3+1 dimensions," *Phys.Rev.* **D72** (2005) 054003, arXiv:hep-ph/0505212 [hep-ph].

[60] A. Rebhan, P. Romatschke, and M. Strickland, "Dynamics of quark-gluon-plasma instabilities in discretized hard-loop approximation," *JHEP* **0509** (2005) 041, arXiv:hep-ph/0505261 [hep-ph].

[61] D. Bodeker and K. Rummukainen, "Non-abelian plasma instabilities for strong anisotropy," *JHEP* **0707** (2007) 022, arXiv:0705.0180 [hep-ph].

[62] J. Berges, S. Scheffler, and D. Sexty, "Bottom-up isotropization in classical-statistical lattice gauge theory," *Phys.Rev.* **D77** (2008) 034504, arXiv:0712.3514 [hep-ph].

[63] A. Rebhan, M. Strickland, and M. Attems, "Instabilities of an anisotropically expanding non-Abelian plasma: 1D+3V discretized hard-loop simulations," *Phys. Rev.* **D78** (2008) 045023, arXiv:0802.1714 [hep-ph].